Power exchange between crossed laser beams and the associated frequency cascade

C. J. McKinstrie and V. A. Smalyuk
Department of Mechanical Engineering, University of Rochester, Rochester, New York 14627
and Laboratory for Laser Energetics, 250 East River Road, Rochester, New York 14623

R. E. Giacone and H. X. Vu
Los Alamos National Laboratory, Los Alamos, New Mexico 87545
(Received 6 May 1996; revised manuscript received 26 July 1996)

The power exchange between crossed laser beams made possible by an ion-acoustic wave is studied, as is the associated frequency cascade. The beam evolution is found to depend sensitively on whether the beams are monochromatic or multichromatic initially, and whether their intersection region lies partially or completely within the plasma. [S1063-651X(97)11601-4]

PACS number(s): 52.40.Nk, 42.65.Es, 52.35.Mw, 52.35.Nx

Stimulated Brillouin scattering (SBS) in a plasma [1] is the decay of a higher-frequency light wave into a lower-frequency light wave and an ion-acoustic wave. There is considerable current interest in the near-forward SBS of one [2,3] and two [4–6] laser beams because of its relevance to inertial-confinement-fusion (ICF) research [7,8].

The indirect-drive approach to ICF [8] involves multichromatic laser beams that overlap as they enter the hohlraum. SBS allows the frequency components of one beam to interact with the frequency components of another beam. Because a power transfer between the beams affects the implosion symmetry adversely, it is important to understand this process.

Consider the interaction of two crossed laser beams (A and B) that have a common carrier frequency ω_0. The ponderomotive force associated with the beams drives an ion-acoustic (sound) wave (grating) of wave vector $\mathbf{k}_s=\mathbf{k}_a-\mathbf{k}_b$ and a frequency $\omega_s=c_s k_s$, as shown in Fig. 1(a). In turn, the grating scatters the laser light from one beam direction to the other. This interaction is governed by [3,6]

$$\partial_\xi A=-i(\omega_e^2/2\omega_0 c)nB, \quad \partial_\eta B=-i(\omega_e^2/2\omega_0 c)n^*A, \tag{1}$$

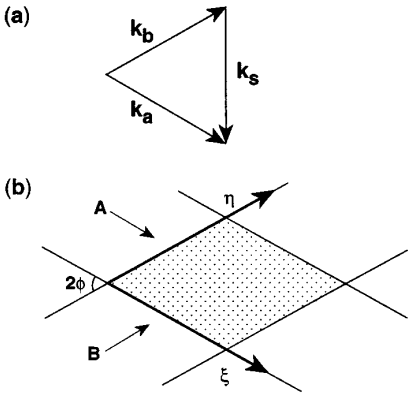

FIG. 1. Geometry of the interaction of crossed laser beams. (a) wave vectors of the laser beams and the ion-acoustic wave. (b) The beam widths are equal and are denoted by w, and the beam intersection angle is denoted by 2ϕ. The characteristic coordinates ξ and η measure distance in the propagation direction of beams A and B, respectively.

$$(\partial_{tt}^2+2\nu_s\partial_t+\omega_s^2)n=-\omega_s^2 AB^*, \tag{2}$$

where $A=(v_a/c_s)(m_e/m_i)^{1/2}$ and $B=(v_b/c_s)(m_e/m_i)^{1/2}$ are the electron quiver velocities associated with the laser fields divided by a characteristic speed that is of the order of the electron thermal speed and n is the electron density variation associated with the grating divided by the background electron density. In Eqs. (1) ξ and η represent distance measured along the propagation directions of the beams, as shown in Fig. 1(b). The time derivatives were omitted from Eqs. (1) because the time taken by the beams to cross the interaction region is much shorter than the time taken by the grating to respond to the ponderomotive force.

Previous studies of the interaction of two crossed laser beams [4–6] assumed that the beams were monochromatic. If the beam frequencies are equal, there is no power transfer in steady state. Conversely, if the beam frequencies differ, in steady state there is a monotonic transfer of power from the higher-frequency beam to the lower-frequency beam.

In this paper we allow the beams to have many frequency components, and study the power transfer between the beams and the associated frequency cascade. For simplicity suppose that each beam has two frequency components with a frequency separation equal to the sound frequency. Subsequently, other frequency components are generated by the interaction, with the same frequency separation that was present initially. One can highlight this frequency cascade by writing

$$A=\sum_j A_j\exp(-\omega_j t), \quad B=\sum_j B_j\exp(-i\omega_j t), \tag{3}$$

where $\omega_j=j\omega_s$, and

$$n=M\exp(-i\omega_s t)+N\exp(i\omega_s t). \tag{4}$$

By substituting definitions (3) and (4) into Eqs. (1) and (2), and making the substitutions $A_j/I^{1/2}\to A_j$, $B_j/I^{1/2}\to B_j$, $(2\omega_s\nu_s/\omega_s^2 I)M\to M$, $(2\omega_s\nu_s/\omega_s^2 I)N\to N$, $\gamma\xi\to\xi$, and $\gamma\eta\to\eta$, where I is the intensity of beam A as it enters the interaction region and $\gamma=\omega_e^2\omega_s^2 I/4\omega_0\omega_s\nu_s c$ is the spatial growth rate of SBS, one can show that

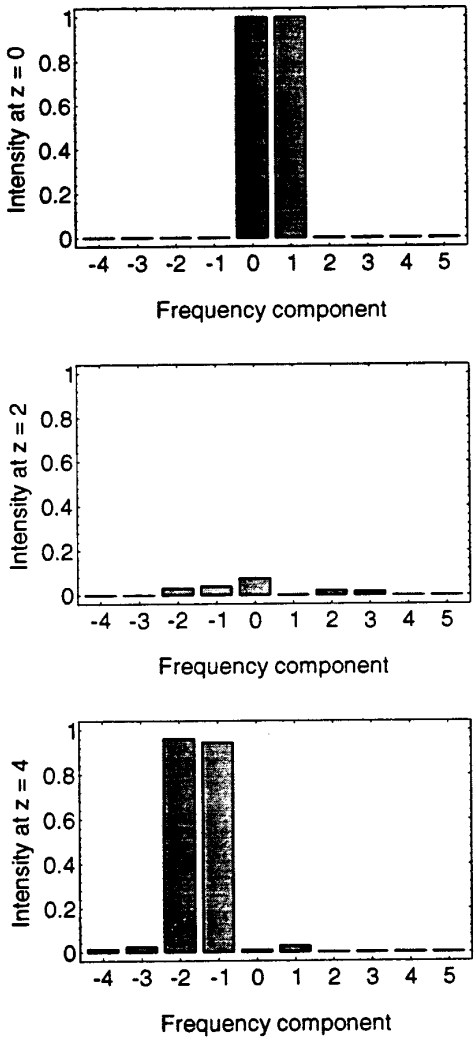

FIG. 2. Frequency spectra of beam A obtained by solving the 1D cascade equations (6) and (7) numerically.

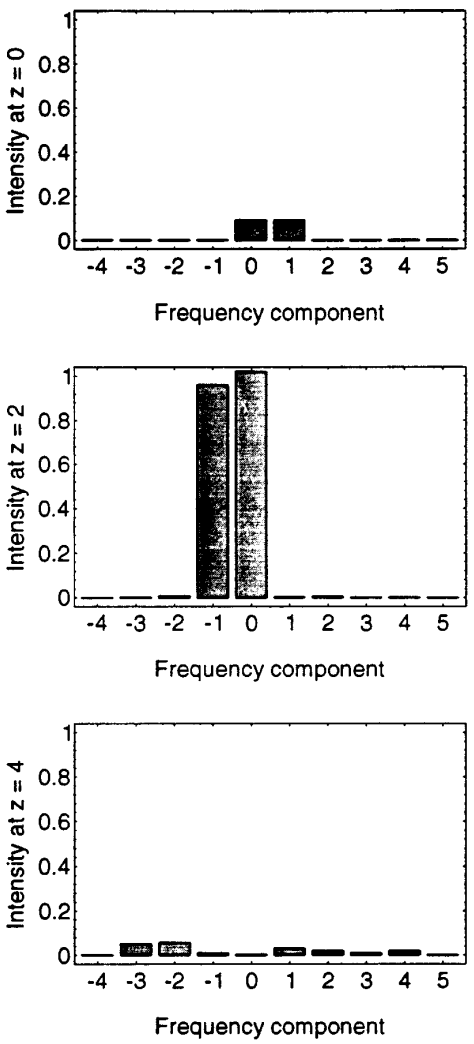

FIG. 3. Frequency spectra of beam B obtained by solving the 1D cascade equations (6) and (7) numerically.

$$d_{\xi}A_j = -i(MB_{j-1} + NB_{j+1}),$$

$$d_{\eta}B_j = -i(N^*A_{j-1} + M^*A_{j+1}), \tag{5}$$

where

$$M = -i\sum_j A_j B_{j-1}^*, \quad N = i\sum_j A_j B_{j+1}^*. \tag{6}$$

The distance variables ξ and η range from 0 to l, where l is the number of SBS gain lengths over which the interaction occurs. The dependence of l on the beam and plasma parameters is discussed in detail in Refs. [4] and [6]. In recent simulations [4] and experiments [9] relevant to ICF, the idealized values of l were 10 and 20, respectively. Although small-scale inhomogeneities of the beams and plasma can reduce the value of l in experiments [9], it is potentially large enough to warrant a detailed study of crossed-beam interactions in ICF.

Because of the intrinsic complexity of the frequency cascade, we began our study with the one-dimensional (1D) equations

$$d_x A_j = -i(MB_{j-1} + NB_{j+1}),$$

$$d_x B_j = -i(N^*A_{j-1} + M^*A_{j+1}), \tag{7}$$

where x represents distance measured along a line that bisects the angle between the ξ and η axes. The 1D cascade equations (6) and (7) are generalizations of equations that arise in the study of beat-wave acceleration [10,11].

A truncated set of 1D cascade equations that allows each beam to have 20 frequency components was solved numerically, subject to the boundary conditions $A_1(0) = A_0(0) = 1$ and $B_1(0) = B_0(0) = \rho$. The intensities of the first ten frequency components of each beam, at discrete distances from the boundary, are displayed in Figs. 2 and 3 for the case in which $\rho = 0.3$. Although the ''microscopic'' evolution of the individual frequency components is complicated, certain trends are evident in the figures. Most of the power contained in beam A is transferred to beam B, then returned to beam A. As power is exchanged, the average frequencies of the beam spectra decrease and the range of frequencies over which power is distributed increases.

Motivated by the apparent periodicity of the power exchange, we plotted the total beam intensities

$$P=\sum_j |A_j|^2, \quad Q=\sum_j |B_j|^2 \tag{8}$$

and the grating strengths

$$R=|M|^2, \quad S=|N|^2 \tag{9}$$

as functions of distance. The evolution of these ''macroscopic'' quantities is displayed in Fig. 4 for the case in which $\rho=0.3$. Despite the complexity of the microscopic evolution, the macroscopic evolution is periodic and predictable. To test the robustness of the observed periodicity, the 1D cascade equations were solved numerically for boundary conditions that included phase shifts between the beams (complex ρ) and between the frequency components of each beam. In all cases the macroscopic evolution was unchanged. This result prompted an analytic analysis of the macroscopic evolution.

It follows from the 1D cascade equations that

$$d_x P=-2(R-S), \quad d_x Q=2(R-S), \tag{10}$$

$$d_x R=2R(P-Q), \quad d_x S=-2S(P-Q). \tag{11}$$

Equations (10) are valid for arbitrary boundary conditions on beams A and B. Terms were omitted from Eqs. (11) that equal zero for the boundary conditions described between Eqs. (7) and (8). There are three conservation laws associated with these model equations. The first is $P+Q=T$, where $T=2+2r$ is the sum of the initial beam intensities and $r=|\rho|^2$. The second is $R+S=U+TQ-Q^2$, where $U=-2r$, and the third is $RS=V$, where $V=r^2$ is the product of the initial grating strengths. By using these conservation laws one cam eliminate R, S, and P from the model equations, which reduce to the potential equation

$$(d_x Q)^2=4Q(Q-2r)(Q-2)(Q-2-2r). \tag{12}$$

It follows immediately that Q oscillates regularly between $2r$, the initial intensity of beam B, and 2, the initial intensity of beam A. As a bonus, Eq. (12) can be solved analytically [12]. The result is

$$Q(x)=2r/[1-(1-r)\mathrm{sn}^2(2x,m)], \tag{13}$$

where $\mathrm{sn}(2x,m)$ is the elliptic sine function of argument $2x$ and order $m=1-r^2$. We verified solution (13) by comparing it to the numerical solution of the 1D cascade equations displayed in Fig. 4(a). It follows from solution (13) that the spatial period of the power exchange

$$l=K(m), \tag{14}$$

where $K(m)$ is the complete elliptic integral of the first kind. For an initial intensity ratio $r=0.09$, $l\approx 3.8$, in agreement with Fig. 4. One can obtain the same result by using the simpler formula $l\approx\ln(4/r)$, which is valid for $r\ll 1$.

In contrast to monochromatic illumination, which results in a monotonic transfer of power from one beam to the other, multichromatic illumination results in a periodic exchange of power between the beams. The main difference between the two cases is the presence of grating N in the latter, which allows energy to be transferred from the higher-frequency components of beam B to the lower-frequency components of beam A. This assertion is supported by Fig. 4(b), in which the growth of grating N after beam A has been depleted is a precursor to the transfer of energy from beam B back to beam A.

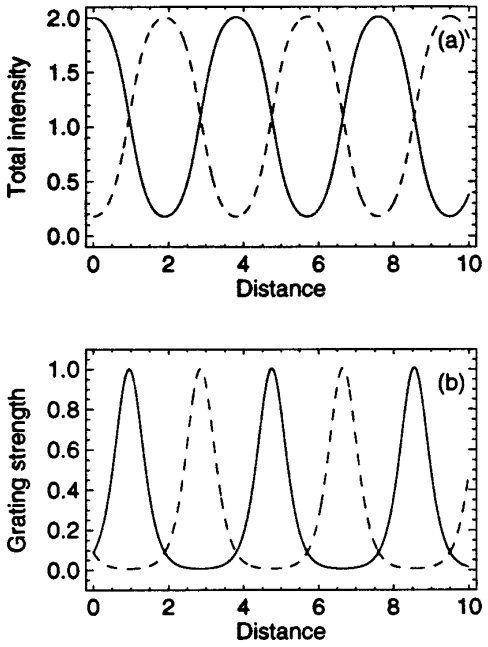

FIG. 4. Periodic evolution of (a) the beam intensities P (solid line) and Q (broken line), and (b) the grating strengths R (solid line) and S (broken line) obtained by solving the 1D cascade equations (6) and (7) numerically.

To test the validity of the preceding 1D results, we integrated the two-dimensional (2D) cascade equations (5) and (6) numerically, subject to boundary conditions that are the 2D analogs of those described between Eqs. (7) and (8). When the beams intersect as they enter the plasma, the interaction region is a triangle. When the beams intersect after they have entered the plasma, the interaction region is a rhombus.

The results for the triangular interaction region are displayed in Fig. 5. Light shading represents high beam intensity and grating strength, whereas dark shading represents low beam intensity and grating strength. The beam and grating evolution is periodic in the x direction, and the growth of grating N is a precursor to the transfer of power from beam B back to beam A, as predicted by the 1D cascade equations. Within the interaction region, the 1D and 2D results agree quantitatively.

The results for the rhomboidal interaction region are displayed in Fig. 6. Clearly, the beam evolution is not periodic in any direction. Although 2D rhomboidal geometry suppressed the periodicity that is characteristic of the 1D and 2D triangular geometries, it does not suppress the effects of multichromatic illumination completely. Under monochromatic illumination $P(\xi,0)=\exp(-2r\xi)$: the intensity of beam A decreases as it propagates near the entry boundary of beam B, as shown in Fig. 4(b) of Ref. [6]. In contrast, under multichromatic illumination $P(\xi,0)=1+\cosh(4r\xi)$: the intensity of beam A increases as it propagates near this boundary, as shown in Fig. 6(a). Once again this qualitative difference is

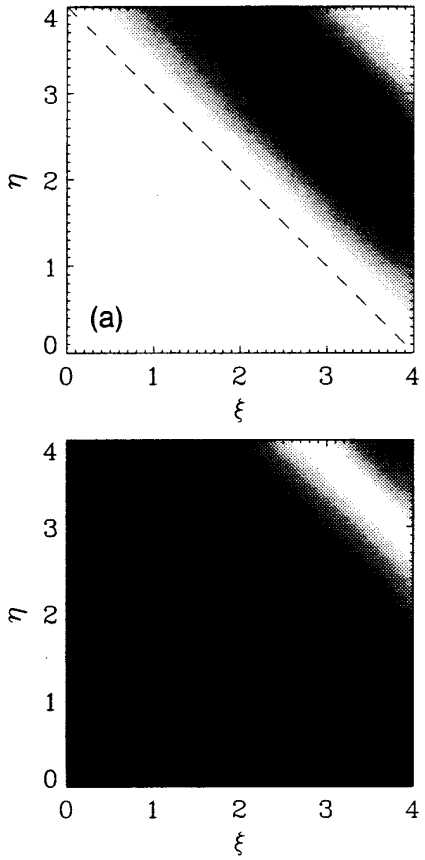

FIG. 5. Gray-scale plot of (a) the total intensity of beam A and (b) the strength of grating N obtained by solving the 2D cascade equations (5) and (6) numerically for a triangular interaction region. The horizontal and vertical axes correspond to the propagation directions of beams A and B, respectively.

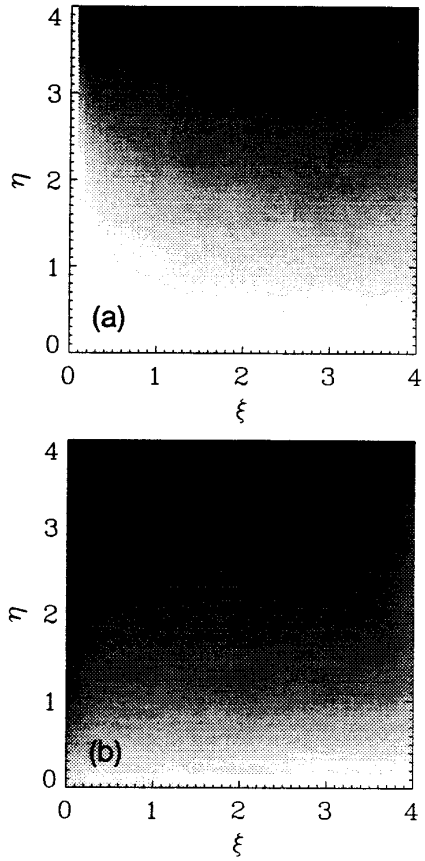

FIG. 6. Gray-scale plot of (a) the total intensity of beam A and (b) the strength of grating N obtained by solving the 2D cascade equations (5) and (6) numerically for a rhomboidal interaction region. The horizontal and vertical axes correspond to the propagation directions of beams A and B, respectively.

due to grating N, which is strong near the aforementioned boundary, as shown in Fig. 6(b).

In summary, the power exchange between two crossed laser beams was studied analytically and numerically. Multichromatic illumination and two-dimensional geometry are both capable of changing the qualitative character of the beam evolution, so their effects should not be overlooked.

This work was supported by the National Science Foundation under Contracts Nos. PHY-9057093 and PHY-9415583, the United States Department of Energy (DOE) under contract No. W-7405-ENG-36, the DOE Office of Inertial Confinement Fusion under Cooperative Agreement No. DE-FC03-92SF19460, the University of Rochester, and the New York State Energy Research and Development Authority. The support of DOE does not constitute an endorsement by DOE of the views expressed in this article.

[1] W. L. Kruer, *The Physics of Laser Plasma Interactions* (Addison-Wesley, Redwood City, California, 1988), Chaps. 7 and 8.
[2] C. J. McKinstrie *et al.*, Phys. Rev. E **50**, 2182 (1994).
[3] R. E. Giacone, C. J. McKinstrie, and R. Betti, Phys. Plasmas **2**, 4596 (1995).
[4] W. L. Kruer *et al.*, Phys. Plasmas **3**, 382 (1996).
[5] V. V. Eliseev *et al.*, Phys. Plasmas **3**, 2215 (1996).
[6] C. J. McKinstrie *et al.*, Phys. Plasmas **3**, 2686 (1996).
[7] R. L. McCrory and J. M. Sources, in *Laser-Induced Plasmas and Applications*, edited by L. J. Radziemski and D. A. Cremers (Dekker, New York, 1989), p. 207.
[8] J. D. Lindl, Phys. Plasmas **2**, 3933 (1995).
[9] R. K. Kirkwood *et al.*, Phys. Rev. Lett **76**, 2065 (1996).
[10] B. I. Cohen, A. N. Kaufman, and K. M. Watson, Phys. Rev. Lett. **29**, 581 (1972).
[11] S. J. Karttunen and R. R. E. Salomaa, Phys. Rev. Lett. **56**, 604 (1986).
[12] C. J. McKinstrie, X. D. Cao, and J. S. Li, J. Opt. Soc. Am. B **10**, 1856 (1993), Appendix A.